Published in final edited form as:
Nat Genet. 2016 November ; 48(11): 1359–1369. doi:10.1038/ng.3681.

TSHZ3 deletion causes an autism syndrome and defects in cortical projection neurons

Xavier Caubit[#1], **Paolo Gubellini**[#1], **Joris Andrieux**[2], **Pierre L. Roubertoux**[3], **Mehdi Metwaly**[1], **Bernard Jacq**[1], **Ahmed Fatmi**[1], **Laurence Had-Aissouni**[1], **Kenneth Y. Kwan**[4,5], **Pascal Salin**[1], **Michèle Carlier**[6], **Agne Liedén**[7], **Eva Rudd**[7], **Marwan Shinawi**[8], **Catherine Vincent-Delorme**[9], **Jean-Marie Cuisset**[10], **Marie-Pierre Lemaitre**[10], **Fatimetou Abderrehamane**[2], **Bénédicte Duban**[11], **Jean-François Lemaitre**[11], **Adrian S. Woolf**[12], **Detlef Bockenhauer**[13], **Dany Severac**[14], **Emeric Dubois**[14], **Ying Zhu**[4], **Nenad Sestan**[4], **Alistair N. Garratt**[15], **Lydia Kerkerian-Le Goff**[1], and **Laurent Fasano**[1]

[1]Aix Marseille Univ, CNRS, IBDM, Marseille, France

[2]Institut de génétique médicale, Hôpital Jeanne de Flandre, CHRU Lille, France

[3]Aix Marseille Univ, INSERM, GMGF, Marseille, France

[4]Department of Neuroscience, Yale School of Medicine, New Haven, CT, USA

[5]Molecular & Behavioral Neuroscience Institute (MBNI), Department of Human Genetics, University of Michigan, Ann Arbor, MI, USA

[6]Aix Marseille Univ, CNRS, LPC, Marseille, France

[7]Karolinska University Hospital Solna, Clinical Genetics Unit, Stockholm, Sweden

[8]Department of Pediatrics, Division of Genetics and Genomic Medicine, Washington University School of Medicine, St. Louis, MO, USA

[9]Service de Génétique clinique, Hôpital Jeanne de Flandre, CHRU Lille, France

[10]Service de Neuropédiatrie, Hôpital Salengro, CHRU Lille, France

Correspondence should be addressed to L.F. (laurent.fasano@univ-amu.fr).

URLs:
The Affymetrix Whole Genome- Human SNP Array 6.0: www.affymetrix.com
MGI GO term finder: www.informatics.jax.org/gotools/MGI_Term_Finder.html
Viewpoint-Behavior technology: www.viewpoint.fr/en/home

Accession codes: GEO accession numbers GSE85512. Our Series record GSE85512 provides access to all of our data and is the accession that should be quoted in any manuscript discussing the data. Raw data (FAstQ files) of the sequencing experiment (triplicate from wild-type and *Tshz3* mutant cortices) and raw abundance measurements of genes (read counts) for each sample are available from GEO.

Author Contributions
X.C., P.G., P.L.R., L.HA., N.S., A.N.G., L.KLG. and L.F. designed the study; X.C., P.G., P.L.R., C.F., J.A., A.N.G., B.J., M.M., L.HA., K.Y..K., P.S. and Y.Z. performed experiments. J.A., A.L., E.R., M.S., C.V.M, J-M.C., M-P.L., F.A., B.D., J-F.L., A.S.W. and D.B. contributed clinical samples and clinical data; A.F., X.C. and L.F prepared RNA samples and D.S. and E.D. produced and performed bioinformatics analysis of RNA-seq data (MGX-Montpellier GenomiX). X.C., P.G., P.L.R., L.HA., P.R., M.C., AN.G., B.J., K.Y.K., N.S., L.KLG. and L.F. analyzed data; X.C., P.G., P.L.R., L.HA., N.S., AN.G., AS. W, L.KLG. and L.F. wrote the paper.

Competing Financial Interests
The authors declare no competing financial interests.

Europe PMC Funders Author Manuscripts

[11]Centre de cytogénétique, Hôpital Saint Vincent de Paul, GHICL, UCL, Lille, France

[12]Institute of Human Development, Faculty of Medical and Human Sciences, University of Manchester, Manchester Academic Health Science Centre and the Royal Manchester Children's and St Mary's Hospitals, Manchester, UK

[13]UCL Institute of Child Health, London, UK

[14]MGX-Montpellier GenomiX, c/o Institut de Génomique Fonctionnelle, Montpellier, France

[15]Institute of Cell Biology and Neurobiology, Center for Anatomy, Charité University Hospital Berlin, Berlin, Germany

[#] These authors contributed equally to this work.

Europe PMC Funders Author Manuscripts

Abstract

TSHZ3, which encodes a zinc-finger transcription factor, was recently positioned as a hub gene in a module of genes with the highest expression in the developing human neocortex, but its functions remained unknown. Here, we identify *TSHZ3* as the critical region for a syndrome associated with heterozygous deletions at 19q12q13.11, which includes autism spectrum disorder (ASD). In *Tshz3* null mice, differentially expressed genes include layer-specific markers of cerebral cortical projection neurons (CPNs) and their human orthologues are strongly associated with ASD. Furthermore, mice heterozygous for *Tshz3* deletion show functional changes at synapses established by CPNs and exhibit core ASD-like behavioral abnormalities. These findings reveal essential roles for *Tshz3* in CPN development and function, whose alterations can account for ASD in the newly-defined *TSHZ3* deletion syndrome.

Autism spectrum disorder (ASD) defines a heterogeneous group of neurodevelopmental disorders that share core behavioral abnormalities, characterized by impairments in social communication and interaction, restricted interests and repetitive behaviors, as defined in DSM-51. ASD has a large genetic component2 and recent integrative genomic analyses have converged on altered fetal development of glutamatergic projection neurons of the cerebral cortex as a possible substrate3–5.

The neocortex is a highly organized laminar structure. Neurons within each layer adopt specific identities and form appropriate local and long-distance connections. The proper formation of these synaptic connections is instrumental for cognitive and motor abilities, and defects in these developmental processes have been associated to ASD6. The different subtypes of cerebral cortical projection neurons (CPNs), distinguished by their molecular, physiological and connectional properties, have characteristic layer distribution. Neuronal positioning and acquisition of laminar and projectional identity are concomitantly controlled by cell type-specific and layer-specific transcriptional programs7. Sequence and copy number variations in the genes encoding key transcription factors modulating neuron positioning and identity, such as FEZF2 (also known as FEZL or ZFP312), SATB2, SOX5 and TBR1, have been found in patients with ASD or disabilities frequently associated with ASD, such as developmental and language delays or intellectual disability (ID)8–11.

Recent spatiotemporal analysis of the human brain transcriptome has positioned *teashirt zinc finger homeobox family member 3* (*TSHZ3*; also known as *ZNF537*) as a hub gene in a module (M8) of co-expressed genes with the strongest levels of expression in early cortical development; "hub genes" being defined as having the highest degree of connectivity, suggesting functional importance, within the module12. The module notably contains *TBR1*, *FEZF2*, *FOXG1*, *SATB2* and *EMX1*, which have been functionally implicated in the development of CPNs13–21. Linkage analysis implicated 19q12 in autism22,23 and a genome-wide association study24 mentioned *TSHZ3* as a potential autism susceptibility gene among 860 candidate genes, but no follow-up study has been performed. These data raise the core question of the role of *TSHZ3* in cortical development and in the pathogenesis of neurodevelopmental disorders. We previously provided evidence that *Tshz3* is required for the proper differentiation and/or survival of a neuronal subpopulation in the developing mouse hindbrain involved in the control of breathing25. As a consequence, $Tshz3^{lacZ/lacZ}$ mice fail to breathe and die at birth. *Tshz3* is also expressed in the developing and adult mouse cortex26, where its function remains unknown.

Here, we identify the gene *TSHZ3* as the minimal region of overlap of 19q12q13.11 heterozygous deletions found in patients with neurodevelopmental disorders. By combining mouse genetics, RNA-seq analyses, electrophysiology and behavioral testing, we provide strong experimental evidence for a causal relationship between *Tshz3* heterozygosity, functional defaults in cortical projection neurons and ASD.

Results

TSHZ3 haploinsufficiency causes neurocognitive impairment

We identified seven new patients from six unrelated families with 19q12q13.11 deletions (Fig. 1a). Patients 1, 2 and 5 have large overlapping deletions (2.4, 4.02 and 2.87 Mb, respectively), defining a minimal region of overlap of 0.83 Mb that encompasses a unique protein-coding gene, *TSHZ3* (Fig. 1a and Table 1). Patients 3a, b, 6 and 7 have smaller deletions (1.0, 0.46 and 0.05 Mb, respectively), which also overlap only *TSHZ3*; the 50 kb microdeletion found in patient 7 deletes the second exon and part of the intron of *TSHZ3*. Interestingly, *TSHZ3* is also deleted in 7 previously reported cases with 19q12q13.1 deletions27–30, 3 of which do not delete the previously described minimal region of overlap on 19q13.11 (Fig. 1a). These 3 literature cases share characteristic clinical features with the 7 cases reported here, including developmental delay (in particular absence or delay of speech), ID, autistic features and renal tract abnormalities, but not microcephaly or ectodermal dysplasia that are unique features associated with the 19q13.11 microdeletion syndrome (Table 1). Notably, among the 22 patients (7 patients in our cohort and 15 previously reported cases) with 19q12q13.11 deletions (Table 1), those diagnosed with ASD (patients 2, 6 and 7 from present study; patient 6 from27 and 5 from28), atypical autism (patient 3a) or ASD-related deficits (1 and 5 from this study) have *TSHZ3* deletion (Fig. 1a and Table 1).

Midfetal human deep cortical layer neurons express TSHZ3

TSHZ3 has been identified as a hub gene in a module (M8) of co-expressed genes with the highest levels in midfetal cerebral neocortex12. We performed a novel analysis of the original spatio-temporal human brain transcriptome data set, using *TSHZ3* as a seed, to identify the 49 genes whose expression profiles show the highest correlation with *TSHZ3* in the developing neocortex. This *TSHZ3* network contains 34 ASD candidate genes, out of which 6 encode transcription factors that are key regulators of CPN identity and connectivity: TBR116,17, FEZF214,18, FOXG113, SATB219,21, SOX531,32 and MEF2C33,34 (Supplementary Fig. 1a,b and Supplementary Table 1). This prompted us to characterize the distribution of the TSHZ3 protein in human midfetal neocortex (i.e., 20 weeks postconception), in comparison with the localization of TBR1 and of BCL11B (also known as CTIP2), which are respective markers of corticothalamic and subcerebral projection neurons17,35. TSHZ3 was detected at the highest levels in L5, where it co-localized with BCL11B, and in L6 and subplate, where it co-localized with TBR1 (Fig. 1b). Since coexpression networks have implicated midfetal L5/L6 CPNs in ASD pathogenesis5, these data support the view that behavioral deficits associated with *TSHZ3* deletion may be related to developmental defects in deep CPNs.

TSHZ3 is expressed in the embryonic mouse neocortex

The 19q12 region where the human *TSHZ3* gene resides is syntenic with the region of the mouse chromosome 7 containing the mouse *Tshz3* gene, and there is a high degree of conservation between *TSHZ3* and *Tshz3*, with 95% amino acid identity in the protein sequences. Similar to the human, at E18.5 in the mouse cortex (equivalent to human midfetal development36), TSHZ3 was detected in postmitotic neurons of L5, L6 and the subplate (Fig. 1c). In the subplate and L6, TSHZ3 was present in TBR1-positive neurons and, within L5, TSHZ3 was detected in BCL11B-positive neurons (Fig. 1c). In contrast to human, TSHZ3 was also detected in L2-3 neurons (Fig. 1c).

Tshz3 deletion alters cortical layer marker gene expression

To identify genes that are regulated by *Tshz3* in the neocortex, we performed RNA sequencing (RNA-Seq) using whole mouse cortex isolated from $Tshz3^{lacZ/lacZ}$ mutants and wild-type controls at E18.5. This analysis identified 243 differentially expressed (DEX) genes among which 116 were down-regulated and 127 were up-regulated ($p<0.05$) in $Tshz3^{lacZ/lacZ}$ mice (Supplementary Table 2). To determine whether some of the DEX genes are expressed in neuronal subtypes and might play functional roles in their development, we integrated information from the literature and several public data sources (DeCoN, Allen Brain Atlas, GenePaint, Eurexpress, the subplate gene expression atlas). This search yielded 23 genes expressed in the subplate, which contains some of the earliest generated neurons and the first functional synapses of the neocortex37, and 144 markers of CPNs, 62 being expressed in all layers and 82 with layer specificity (Fig. 2a and Supplementary Table 3). These latter include 52 markers of deep layer cortical neurons, 12 being specific to L5 (subcerebral projection neurons) and 27 specific to L6 (corticothalamic neurons) (Fig. 2b). Interestingly, 11/12 (91.6%) of the L5 markers were up-regulated and 23/27 (85.1%) of the L6 markers were down-regulated (Fig. 2b and Supplementary Table 3), indicating that *Tshz3*

mutation profoundly alters the gene-expression properties of deep layer cortical neurons. In order to identify the biological processes in which TSHZ3 may be involved in the mouse cortex, we performed a pathway analysis of the 211 protein-coding genes out of the 243 DEX genes using the PANTHER database38. Whereas only 9% of all mouse protein-coding genes (2,070/22,275) are components of the 150 PANTHER regulatory pathways, 19% of the DEX protein-coding genes (40/211) were involved in as much as 63 of these pathways. More specifically, out of the 49 brain and general development pathways encoded by the mouse genome, 39 (79.5%) were represented among DEX genes, with an enrichment for pathways related to neurotransmitter/neuropeptide receptor signaling ("metabotropic glutamate receptor", "5HT1-4 type receptor mediated signaling pathway"…). Gene ontology (GO) analysis was performed for the 144 DEX genes categorized as CPN markers, considering separately the 52 deep CPN-specific genes and the others. GO terms related to neuron and axon development ("axogenesis", "cell morphogenesis involved in neuron differentiation", "neuron projection development"…) were identified among the most significant categories for the deep CPN-specific genes, specifically. These data suggest regulatory functions for TSHZ3 in cortical circuit development (Supplementary Table 4).

qRT-PCR for 14 DEX genes representative of different expression profiles (*Fgf10* for L5, *Fezf2* and *Nr4a1* for L5/6, *Ramp3* for L6, *Col23a1, Gdf10, Gsg1l*, *Hs3st3b1, Hs3st4, Igfbp3, Ngfr* and *Stac2* for L6/subplate and *Col5a1* and *Cplx3* for subplate) validated RNA-seqdata by showing 100% concordance (Fig. 2c and Supplementary Fig. 2a,b). *In situ* hybridization (ISH) or immunocytochemistry, which gave reliable signal for 10 of these selected DEX genes, also confirmed the RNA-seq data and further provided information on the layer specificity of the molecular changes (Fig. 2c and Supplementary Fig. 2b). In addition, ISH for *Fgf10, Ngfr, Col5a1* and *Igfbp3* revealed spatial caudo-rostral variations for DEX genes, consistent with the gradient of *Tshz3* expression (Supplementary Fig. 2b,c). Accordingly, the DEX gene list included previously identified caudal markers (*Dkk3, Crym, Tshz2, Bhlhe22, Ngfr*)17, and five additional genes were categorized here as caudal markers based either on a search in gene expression databases (*Col5a1, Gdf10, Flrt1, Igfbp3*) or on the present ISH data (*Fgf10*).

Tshz3 deletion modifies ASD-associated gene expression

Since 232 of the 243 mouse DEX genes have a non-ambiguous human ortholog, we reasoned that examining their disease association could represent a valuable clue as to TSHZ3 function. Extensive PubMed searches for all DEX genes human orthologs identified 157/232 genes (67.7%), which are established or putative cause for brain and/or nervous system disorders. Interestingly, the great majority of these genes (110/157; 70.1%) has been associated with ASD, the second most represented disease (20.4%) being schizophrenia (Supplementary Table 5). Among the orthologs of the 52 DEX genes expressed in L5/6, these percentages were 61% for association with ASD and 27% for association with schizophrenia (Fig 2d). Since recent studies associated deep layer CPNs to neurodevelopmental pathologies, including autism and schizophrenia5,36, our analyses point to TSHZ3 as a nexus in a brain developmental gene network whose defects are associated with these disorders.

Tshz3 deletion preserves cortical layering and projections

To investigate potential changes in cortical layering and neuronal density in *Tshz3*$^{lacZ/lacZ}$ mutants, we analyzed at E18.5 the expression of classical layer-specific markers for CPNs: SATB2, BCL11B, SOX5, TBR1 and TLE4, whose genes were not among the DEX genes. *Tshz3*$^{lacZ/lacZ}$ mutants showed normal expression of these 5 markers (Fig. 3a), indicating that, despite altered molecular identity, cortical layering was unaffected by *Tshz3* deletion. No significant differences in cell numbers in L5 and in L6 were found in *Tshz3*$^{lacZ/lacZ}$ mutants in comparison to wild-type mice, when quantifying respectively the numbers of BCL11B-positive (33.94 ± 1.55 vs. 33.10 ± 2.23; p=0.7561), and TBR1-positive cells (93.45 ± 3.19 vs. 87.14 ± 3.22; p=0.1705) (cells/100 μm; n=28 sections from 3 animals per genotype).

To investigate whether the differential gene expression by deep layer neurons in *Tshz3* mutant is associated with changes in axon pathfinding, we immunostained coronal sections of E18.5 *Tshz3*$^{lacZ/lacZ}$ brains for neurofilament (NF) and the axonal marker L1-cam, and compared them to sections from wild-type brains. We found that *Tshz3*$^{lacZ/lacZ}$ brains displayed no gross defects in major axon tracts (Fig. 3b,c).

Tshz3 haploinsufficiency alters neocortical gene expression

Heterozygous *Tshz3* deletion that genetically mimics the *TSHZ3* patient condition is expected to provide data relevant to processes underlying the human syndrome. The *Tshz3*$^{+/lacZ}$ heterozygous mice showed decreased neonatal viability25,39 (100% lethal on C57BL/6J background and 50% on CD1 [Crl:CD1 (ICR); Charles River] or CBA/H GNC background), but otherwise they remain poorly characterized. Consistent with the association of *Tshz3* deletion with renal tract defects (100% of *Tshz3*$^{lacZ/lacZ}$ homozygous mice had bilateral hydroureter)39, about 1/4 of heterozygous embryos from E16.5 onwards presented unilateral hydroureter (26.8%; 19/71).

We tested whether such heterozygosity altered the expression of DEX genes identified at E18.5 in *Tshz3*$^{lacZ/lacZ}$ cortex. We addressed this question using qRT-PCR for the 14 DEX genes previously selected for the validation of RNA-seq data. In *Tshz3*$^{+/lacZ}$ mice at E18.5, significant up or down-regulations *vs.* wild-type were found for 10 of them, as in *Tshz3*$^{lacZ/lacZ}$ mutants: *Col5a1, Col23a1 Cplx3*, *Fgf10, Gsg1l, Hs3st3b1, Hs3st4*, *Igfbp3*, *Ngfr, Ramp3* (Fig. 4a). At P5, the expression of five genes was also modified in *Tshz3*$^{+/lacZ}$ mice *vs.* wild-type, similarly to *Tshz3*$^{lacZ/lacZ}$ mutants: *Cplx3, Fgf10, Gsg1l, Igfbp3*, *Ramp3* (Fig. 4a). At P20, two were differentially expressed in *Tshz3*$^{+/lacZ}$ mice *vs.* wild-type as in *Tshz3*$^{lacZ/lacZ}$ mutants (*Nr4a1, Ramp3*), while 4 were inversely regulated (*Col5a1, Col23a1, Gdf10, Igfbp3*) (Fig. 4a). These results show that *Tshz3* haploinsufficiency induces a complex temporal dynamic of molecular changes from embryonic to postnatal stages, presumably affecting the maturation/differentiation of cortical neurons.

Tshz3 haploinsufficiency alters synaptic function

Defects in the corticostriatal circuit have been implicated in ASD-like behaviors40. In the mouse, corticostriatal projection neurons are mostly located in L5 and their axons reach the striatum at P3-P441, where they start forming synapses from P10 onwards. Their main

targets are the dendritic spines of medium-sized spiny neurons (MSNs), which constitute more than 90% of the whole striatal population and are projection neurons. In wild-type postnatal brains, TSHZ3 was expressed in corticostriatal neurons (Fig. 4b) but not in MSNs; the few striatal TSHZ3-positive neurons were not positive for BCL11B, which is enriched in MSNs (Fig. 4b)42, and are thus likely interneurons.

We used the corticostriatal circuit as a model system to investigate the presence and functionality of CPNs in *Tshz3*$^{+/lacZ}$. Dual retrograde tract-tracing from the dorsal striatum and from the thalamus using two different cholera toxin subunit B-conjugated fluorophores demonstrated that the corticostriatal projections from L5 CPNs and the corticothalamic projections from L6 CPNs were present in *Tshz3*$^{+/lacZ}$ mouse brains as in wild-type (Fig. 4c).

To analyze corticostriatal synaptic transmission, we performed slice electrophysiological recordings of MSNs in the dorsolateral striatum (Fig. 5a). Resting membrane potential, action potential (AP) discharge, input resistance and current-voltage relationship of MSNs were similar in wild-type and *Tshz3*$^{+/lacZ}$ mice (Supplementary Fig. 3). However, paired-pulse ratio (PPR) of AMPA receptor-mediated excitatory postsynaptic currents (EPSCs), evoked by electrical stimulation of corticostriatal fibers, was lower in MSNs from *Tshz3*$^{+/lacZ}$ mice (Fig. 5b). This suggests an increased probability of AP-dependent glutamate release from CPNs of heterozygous mice. Spontaneous miniature EPSCs (mEPSCs) recorded in the presence of tetrodotoxin were similar in wild-type and *Tshz3*$^{+/lacZ}$ mice, in terms of both frequency (Fig. 5c) and amplitude (Fig. 5d). These data suggest, respectively, that AP-independent glutamate release from CPNs is not affected by heterozygous *Tshz3* loss and that the sensitivity of AMPA receptors located on striatal MSNs is unchanged. Accordingly, the AMPA/NMDA receptor ratio was similar in *Tshz3*$^{+/lacZ}$ mice compared to wild-type (Fig. 5e). Finally, we observed that corticostriatal long-term potentiation (LTP) was present in both wild-type and heterozygous mice, but was significantly enhanced in the latter (Fig. 5f).

Tshz3 haploinsufficiency results in autism-like behavior

Unless otherwise mentioned, *Tshz3*$^{+/lacz}$ male mice on a CBA/H/Gnc x CD1 F1 background were used for behavioral studies. We verified that these animals did not show visual, auditory or olfactory deficits (Supplementary Fig. 4). We then investigated whether *Tshz3* haploinsufficiency resulted in ASD-like traits by measuring the two core features, i.e., impairment of social interactions and stereotyped repetitive behaviors with restricted interests, that serve to diagnose ASD (DSM-5)1. The first criterion was evaluated using a two-chamber device43 and a protocol we adapted44 (Fig. 6a) from the three-chamber test 45,46. Wild-type and *Tshz3*$^{+/lacZ}$ did not significantly differ in exploration of empty boxes during the habituation stage (Fig. 6b). Unlike wild-type, *Tshz3*$^{+/lacZ}$ mice did not interact more frequently with a conspecific than with an empty box containing a lure (sociability) (Fig. 6c) and they did not display more interaction with a “novel” *vs.* a “familiar” conspecific (preference for social novelty) (Fig. 6d). Similar results were obtained when examining mice with CD1 background and using the three-chamber test45,46 (Supplementary Fig. 5), which confirmed the robustness of the gene haploinsufficiency

impact on social functioning. The second criterion (restricted, repetitive patterns of behavior) was assessed in three independent tasks. The marble-burying test showed a repetitive pushing and digging activity in the *Tshz3*$^{+/lacZ}$ mice (Fig. 6e). In the hole-board, *Tshz3*$^{+/lacz}$ mice made a total number of nose dips similar to wild-type. But when considering separately exploratory and stereotyped dips as previously defined47,48, *Tshz3*$^{+/lacz}$ mice performed a higher number of stereotyped dips (Fig 6f, g). In the open-field, while the total distance walked was similar in the two genotypes (Fig 6h), the number of zone crossings was lower in the *Tshz3*$^{+/lacZ}$ (Fig 6i), indicating a reduced field of interest. All the differences were characterized by an effect size that was large enough to be considered as being in the range of the pathological variation49. Since anxiety has a high prevalence in ASD50, we also measured anxiety-like behavior. *Tshz3*$^{+/lacZ}$ mice avoided the central zone of the open-field (Fig. 6j) and, in an elevated plus-maze, while travelling similar total distance (Fig. 6k), they travelled less in the open arms (Fig. 6l), which indicates a higher anxiety-like behavior. The body mass was smaller in *Tshz3*$^{+/lacZ}$ than in wild-type mice, but it did not reach the significance at the age of the experiment [(35.25 ± 2.10 g vs. 36.58 ± 1.96 g) for Fig. 6b-d and (36.01 ± 2.08 g vs. 37.18 ± 1.81 g) for Fig. 6e-l] and it never impacted the different behaviors when it was used as covariate (Supplementary Table 6). Together, the analyses indicated that *Tshz3* haploinsufficiency resulted in ASD-like phenotype.

Discussion

In the present study, we identified the *TSHZ3* gene as the smallest region of overlap of 19q12q13.11 deletions in a new cohort of 7 patients and in 7 previously reported subjects27–30. The characteristic clinical features encompass neurodevelopmental disorders, including autistic traits, speech disturbance and intellectual disability, as well as renal tract abnormalities. Most deletions were *de novo*, supporting their association with the new syndrome described. Reduced penetrance can explain the inheritance of the deletion from unaffected parents. The autistic features presented by the patient who has the smallest (50 kb) deletion involving only the *TSHZ3* gene lead to consider *TSHZ3* as the gene of interest responsible for the neurocognitive phenotype of these patients. Thus, our data validate the GWAS-identified *TSHZ3* gene24 as an ASD risk gene. A possible explanation for the scarcity of studies that have associated *TSHZ3* with ASD could be that *TSHZ3* is a dosage-sensitive gene whose haploinsufficiency is linked to high developmental lethality. In mice, *Tshz3* heterozygosity is 50% lethal on CD1 background25 and 100% on C57BL/6J background39. We thus speculate that *TSHZ3* mutations define an ASD subtype characterized by the clinical association of autistic features with other syndromic features, especially genito-urinary tract defects. Importantly, such an association should help identifying additional *TSHZ3* patients. The link between *TSHZ3* deletion and this newly reported syndrome is strengthened by the studies in the mouse. For instance, *Tshz3*/*TSHZ3* is expressed at key stages of the developing metanephros51 and neocortex in mouse as in human, and *Tshz3* mutation in the mouse recapitulates features of the human phenotype: hydroureter and ASD-relevant behavioral abnormalities. Interestingly, mutations in several genes have been associated with complex phenotype including both ASD features and renal tract abnormalities52–55.

There is strong evidence for spatiotemporal convergence among groups of disease-related mutations, all known to lead to ASD, in midfetal L5/6 glutamatergic CPNs5. Interestingly, our coexpression network analysis of the developing human neocortex using *TSHZ3* as a seed identified 34 ASD candidate genes among the 49 genes with highest correlation to *TSHZ3*, including *TBR1*, *FEZF2* and *SOX5*. Moreover, 5 out of the 49 *TSHZ3*-connected genes in the human module are differentially expressed in *Tshz3*$^{lacZ/lacZ}$ mice and have been associated to ASD: *FEZF2*, *KLHL1*, *PRDM8*, *SLA* and *SLC44A5* (Supplementary Fig. 1a). These data provide support to the hub position of *TSHZ3* in a cortical transcriptional regulatory network associated with ASD.

Our study in the mouse, by showing gene expression variation in the cerebral cortex, enrichment of ASD-related genes in orthologs of DEX genes, functional alteration in neural circuit formed by CPNs and behavioral abnormalities associated with *Tshz3* deficiency, provide some clues on the link between *TSHZ3* deletions and ASD.

During prenatal development, we found that *Tshz3* function is dispensable for cortical layering but required for normal expression of marker genes of subplate and deep layer cortical neurons, with enrichment for GO terms related to neuron and axon development when considering DEX genes categorized as deep CPN markers. In particular, the cortex of *Tshz3*$^{lacZ/lacZ}$ mice showed increased expression of *Fezf2* in L6. Knowing that *Fezf2* is normally down-regulated in L6 while being maintained at high level in L5 at the end of embryogenesis14,18, it can be suggested that high *Fezf2* expression is aberrantly retained in L6 neurons in *Tshz3*$^{lacZ/lacZ}$ mutant cortex, as reported previously in *Sox5*$^{-/-}$ 31,32 and *Tbr1*$^{-/-}$ 16 mice neocortex. *Tshz3* deletion also phenocopies the gene expression changes reported in *Tbr1* mutant for *Bhlhe22* (also known as *Bhlhb5*), *Crym, Pcdh20, Ngfr* and *Tshz2*17, suggesting that *Tshz3* may contribute to TBR1-dependent regulatory mechanism. However, contrarily to what has been observed in *Tbr1*16 and *Sox5*31 mutants, we found that axon pathfinding is preserved in *Tshz3* mutants at E18.5, suggesting that *Tshz3* may rather participate in the postnatal functional maturation of circuits formed by CPNs. This is consistent with the PANTHER analysis of DEX genes in these mutants showing enrichment for pathways related to neurotransmitter/neuropeptide receptor signaling. Perinatally in the mouse, axons from layer 5 CPNs of all cortical areas project towards the spinal cord and, from P0 to P6, they form a similar set of collaterals56. Then, between P6-P14, axon branches are selectively eliminated in an area-specific manner56. While defects in either collateral formation, selective branch elimination and/or synapse refinement might occur in *Tshz3* mutant, the early neonatal lethality of *Tshz3*$^{lacZ/lacZ}$ makes it currently difficult to test this hypothesis. In the subplate, a highly dynamic sector of the developing neocortex, we observed altered expression of *Fezf2* and *Ngfr,* which are critical for corticofugal connectivity and for giving information to thalamocortical incoming connections, respectively14,15. It is noteworthy that genes expressed in a subplate-specific manner during development show a statistically significant enrichment for association with ASD and schizophrenia37.

Interestingly, *Tshz3*$^{+/lacZ}$ mice, which closely model the condition of patients with heterozygous *TSHZ3* deletion, also show altered gene expression in the embryonic and post-natal cortex, and their behavioral phenotype includes the two clinical traits characterizing

ASD according to DSM-51: they display both poor sociability and poor interest in social novelty, not imputable to sensory deficits, and fulfill the restricted field of interest and repetitive behavior condition. The altered gene expression in the post-natal cortex of *Tshz3*$^{+/lacZ}$ mice suggests that post-natal defects in CPN development or function can contribute to the ASD-like phenotype linked to *Tshz3* heterozygosity. There is substantial evidence associating the corticostriatal circuitry with ASD40,57 and changes in corticostriatal function, although heterogeneous, have been evidenced in mouse ASD models, such as knock-outs for *Shank3*58 or *neuroligin-1*59 and in *16p11*$^{+/-}$ mice60. Here we provide evidence for altered corticostriatal synaptic transmission (increased AP-dependent glutamate release) and plasticity (enhanced LTP) in *Tshz3*$^{+/lacZ}$ mice, suggesting increased functional corticostriatal connectivity, consistent with functional imaging data from ASD patients57. The results from our mouse model thus reinforce the gene/phenotype relationship between *TSHZ3* haploinsufficiency and autistic features we evidenced in patients with *TSHZ3* deletion.

This study, from human to rodent model, identifies *TSHZ3*/*Tshz3* as a novel gene linked to ASD, essential for CPN development and function. Its deletion affects the cortical expression of a number of genes related to ASD and induces ASD-relevant deficits, associated with functional changes at synapses formed by deep layer CPNs without obvious alterations in neuron viability, layering and pathfinding. Our data point to TSHZ3 as a key member of a transcriptional regulatory network whose alteration at different nodes (such as TBR1, FEZF2, SATB2) can lead to a convergence of brain phenotypes centering on ASD, and to murine *Tshz3* mutants as novel candidate animal models of ASD.

Online Methods

Consent and human ethics approval

All subjects or their legal representatives gave written informed consent for the study. The present work used only unlinked anonymized data and was performed in accordance with the declaration of Helsinski protocols and approved by the FRANCE, SWEDEN and USA ethics committees. The clinical cytogenetic sample consisted of patients referred to “France, Sweden, USA” from regional pediatricians, other health specialists and/or genetics centers. DNA from subjects was extracted from peripheral blood lymphocytes by standard extraction procedures.

Identification and mapping of deletions in 19q12q13.11

DNA concentration was measured with a NanodropTM spectrophotometer. The Agilent CGH array 60K was used for patients 1 and 2, 44K for patients 5 and 7 and 180K for patients 3a, 3b and parents (Agilent Technologies, Santa Clara, CA). Female or male genomic DNA was used as a reference in sex-match hybridization and results were analyzed with the CGH Analytics, CytoGenomics and Feature Extraction softwares (Agilent Technologies, Santa Clara, USA) and CytoSure Interpret software (Oxford Gene Technology, Oxfordshire, UK). To confirm deletion and check parents’ genome for carrier status (patients 1, 2, 4, 5 and 7), qRT-PCR was performed using the LightCycler480 SYBRgreen I Master chemistry on a LC480 apparatus (Roche, Basel, Switzerland) and data

analyzed using the LightCycler 480 software. The Affymetrix Genome-Wide Human SNP Array 6.0 was used for patient 6. Copy number analysis was performed using the Affymetrix Genotyping Console Software.

Mouse strains

In all the experiments, wild-type littermates were used as control. The *Tshz3*^{lacZ} mouse line has been described previously39. Experimental procedures have been approved by the "Comité National de Réflexion Ethique sur l'Expérimentation Animale n°14" (ID number 57-07112012) and were in agreement with the recommendations of the European Communities Council Directive (2010/63/EU).

Histology

Fluorescence immunocytochemistry—Human fetal brains at 19 and 20 weeks of post-conception were obtained from the Human Fetal Tissue Repository of the Albert Einstein College of Medicine under the guidelines approved by the Yale Institutional Review Board. They were fixed by immersion in 4% paraformaldehyde (PFA) for 36 h, cryoprotected, frozen, and cryosectioned at 60 μm. For immunostaining, brain sections were prepared as previously published31.

Mouse brains were dissected and fixed for 2 h in 4% PFA, cryoprotected overnight in PBS/20% sucrose, embedded in OCT, and cryostat (Leica CM 3050S) sectioned at 16 or 20 μm. Sections were incubated overnight at 4 °C with primary antibodies. L1-cam and neurofilament immunostaining was performed on 100 μm thick vibratome (Leica) sections processed for free floating and standard protocol. Primary/secondary antibodies and dilutions used are detailed in Supplementary Table 7. Images were acquired using a laser scanning confocal microscope (LSM780; Carl Zeiss) and processed using Adobe Photoshop.

Retrograde tracing—P28-old mice under xylazine/ketamine anesthesia received stereotaxic injections of 0.3 μl of Cholera Toxin Subunit B (CT-B, 1 mg/ml; Thermo Fisher Scientific) conjugated with Alexa-Fluor 488 in the striatum (A: +1 mm L:+1.8 mm DV: -2.9 mm from dura), and conjugated with Alexa Fluor 647 in the thalamus (A: -1.3 mm L: +1.15 mm DV: -3.5 mm from dura) using the bregma coordinates61. This allowed retrograde labeling of, respectively, L5 CPNs (striatal injection) and L6 CPNs (thalamic injection). At 10 days post-injection, animals were perfused transcardially with 4% PFA.

***In situ* hybridization—**In situ hybridization was performed on 16 μm cryostat sections as previously described26, or on 80-100 μm thick vibratome (Leica) sections. Vibratome sections were pretreated with 10 μg/ml proteinase K for 5 min, hybridization and post-hybridization washes were done at 70 °C. Probes used are detailed in Supplementary Table 7. Signal was detected with alkaline phosphatase-conjugated anti-DIG antibody and nitro blue tetrazolium chloride/bromo-4-chloro-3-indolyl phosphate (NBT/BCIP) (Roche Applied Science).

Europe PMC Funders Author Manuscripts

Building of *TSHZ3* gene co-expression network

The co-expression network of *TSHZ3* was created using a published microarray data set, including samples from 1,340 tissue samples collected from 16 brain regions of 57 developing and adult healthy donors. A full description of tissue acquisition and processing, data generation, validation and analyses, has been provided12. We used *TSHZ3* as a seed and we selected 49 genes with the highest correlation to *TSHZ3*. The network was created using VisANT, with nodes representing genes and edges representing pairwise correlation between genes. We set the cut-off of correlation > 0.7 for edges; i.e., only genes with correlation greater than 0.7 are connected.

Molecular analyses

RNA sequencing analysis—Three independent replicates, each containing cortices from 3-4 embryos from multiple litters, were prepared from wild-type and *Tshz3* mutant neocortex at E18.5. RNA-Seq libraries were constructed from 1 μg of total RNA with the Truseq stranded mRNA sample preparation kit (Low throughput protocol) kit from Illumina. After poly-A based mRNA enrichment (poly-T oligo attached magnetic beads) and mRNA fragmentation (using divalent cations under elevated temperature), RNA fragments were copied into first strand cDNA using reverse transcriptase and random primers; the second strand cDNA was synthesized subsequently. These cDNA fragments were added with a single 'A' base and then ligated with the adapter. The products were purified and enriched with 15 cycles of PCR. The final cDNA libraries were validated with a DNA 1000 Labchip on a Bioanalyzer (Agilent) and quantified with a KAPA qPCR kit. For one sequencing lane, six libraries were pooled in equal proportions, denatured with NaOH and diluted to 7 pM before clustering. Clustering and 50 nt single read sequencing were performed according to the manufacturer’s instructions.

Image analysis and basecalling were performed using the HiSeq Control Software and Real-Time Analysis component. Data quality was assessed using fastqc from the Babraham Institute and the Illumina software SAV (Sequence Analysis Viewer). Demultiplexing was performed using Illumina's sequencing analysis software (CASAVA 1.8.2). TopHat 2.0.9, a splice junction mapper62 (using Bowtie 2.1.063), was used to align RNA-Seq reads to mouse genome (mm10) with a set of gene model annotations (genes.gtf downloaded from UCSC on March 6 2013). Final read alignments having more than 3 mismatches were discarded. Then, the counting was performed with HTSeq count 0.5.3p9 (union mode). The data is from a strand-specific assay and the read has to be mapped to the opposite strand of the gene. Before statistical analysis, genes with less than 15 reads (cumulating all the analysed samples) were filtered and thus removed. DEX genes were identified using the Bioconductor package DESeq2 1.2.5. and the package edgeR 3.4.0., as genes with adjusted p-value<0.05, according to the false discovery rate method from Benjamini-Hochberg.

Database and bioinformatics analyses

In order to provide insight into the analyses of the 243 DEX genes, relevant information was extracted from several literature, disease or molecular databases: PubMed, SFARI, OMIM and PANTHER. The first three databases were used to characterize the brain and nervous system diseases associated to human orthologs of mouse DEX genes. Extensive Pubmed

searches on each of these genes were performed between September 2015-April 2016 and all clinical brain/nervous system disorders observed in patients harboring mutations in each of the 232 orthologs of mouse DEX genes were noted (Supplementary Table 5). All 806 genes contained in the human module of the SFARI autism database64 were extracted and the SFARI genes common to the orthologs of mouse DEX genes were conserved (Supplementary Table 5). Finally, among the 232 human orthologs of mouse DEX genes, all genes for which a clear genotype-phenotype relationship is described in the human genetic OMIM database were also noted (Supplementary Table 5).

The PANTHER database version 9.0 was used to characterize the regulatory pathways in which some of the DEX genes are engaged (Supplementary Table 4).

Finally, a GO term enrichment analysis was performed using the MGI GO term finder in order to functionally compare, within the mouse DEX genes, those specific of cortical L5-L6 layers to those expressed in L2-L6 layers (Supplementary Table 4).

Quantitative RT-PCR

Total RNA from wild-type and *Tshz3* mutant brains at E18.5 was prepared using Rneasy Plus Universal Mini Kit gDNA eliminator (Qiagen™) and first strand cDNA was synthesized using iScript Reverse Transcription Supermix kit (Bio-RAD™). Real-time PCR was performed on a CFX96 QPCR detection system (Bio-RAD™) using SYBR® GreenER™ qPCR SuperMixes (Life Technologies™). RT-qPCR conditions: 40 cycles of 95 °C for 15s and 60 °C for 60 s. Analyses were performed in triplicate. Transcript levels were first normalized to the housekeeping gene *Gapdh*, and then normalized to their respective control group. Primer sequences used for Sybr qPCR are listed in Supplementary Table 8. Statistical analysis was performed by unpaired *t*-test by using the qbasePLUS software version 2 (Biogazelle). A p- value <0.05 was considered to be significant.

Ex-vivo electrophysiology

Tshz3$^{+/lacZ}$ and wild-type F1 littermates obtained by crossing CD1 *Tshz3*$^{+/lacZ}$ males with CBA/H GNC females were used for electrophysiological recordings. Corticostriatal slices (250 μm) were obtained from brains at P21-28 as described previously65. MSNs of the dorsolateral striatum were identified by infrared videomicroscopy and by their electrophysiological properties66, and were recorded by borosilicate micropipettes (whole-cell patch-clamp, 5-6 MΩ) filled with an internal solution containing (in mM): 125 K-gluconate, 10 NaCl, 1 $CaCl_2$, 2 $MgCl_2$, 0.5 BAPTA, 19 HEPES, 1 Mg-ATP and 0.3 Na-GTP, pH 7.3. For NMDA/AMPA ratio experiments67, it contained (in mM): 140 CsCl, 10 NaCl, 0.1 $CaCl_2$, 10 HEPES, 1 EGTA, 2 Mg-ATP and 0.5 Na-GTP. All recordings were performed in the presence of 50 μM picrotoxin. A tungsten bipolar electrode was placed in the dorsal *corpus callosum* to evoke EPSCs, while spontaneous miniature EPSCs (mEPSCs) were recorded in the presence of 1 μM tetrodoxin. LTP induction protocol consisted in three stimulation trains (100 Hz) of 3 s duration during which the neuron was depolarized to -10 mV, each train separated by a 20 s interval. Electrophysiological data were obtained by an AxoPatch 200B amplifier (Molecular Devices, USA) and analyzed offline by Clampfit 10.2 (Molecular Devices, USA) and MiniAnalysis 6.0 (Synaptosoft, USA). Statistical analysis

was performed by Prism 5 (GraphPad, USA) software. Sample sizes, p values and statistical tests are indicated in Fig. 5 and Supplementary Fig. 3.

Behavioral testing

Unless otherwise mentioned, the *Tshz3*$^{+/lacZ}$ and the wild-type mice were F1 littermates obtained by crossing CD1 *Tshz3*$^{+/lacZ}$ males with CBA/H GNC females. Only the males were subjected to the experimental tasks, at 80-90 days of age. Each male was singly housed with a female in a physically-enriched environment from weaning until testing. Interest in social interactions was evaluated using a two-chamber social approach, restricted field of interest and repetitive behavior using the hole-board, open-field and marble burying tests, as described in44, and anxiety-like behavior using the open-field and elevated plus-maze. All the behavioral evaluations were scheduled between 10am-3pm, with low light (60-70 lux on the ground), except open-field (150 lux), by experimenters blinded to genotype.

We performed parametric analysis with *Statistical Package for the Social Science version 19 (SPSS*)68. ANOVA for repeated measures was used for sociability and preference for social novelty with paired *t* for partial comparisons. Student *t* served for comparisons in the other tasks. ANCOVA served to partial out weight or general activity. The size of the effect was calculated for each inferential result 49.

Sociability and social novelty preference test—The sociability (number of interactions towards a conspecific) and the interest in social novelty (increased number of interactions towards an unknown conspecific, i.e a new arrival) were measured in the *Tshz3*$^{+/lacZ}$ and wild-type male mice according to the principles of the three-chamber test45,46 but in a different two-chamber set up43,44, with opaque walls, as shown in Fig. 6a. The behavior was video recorded via a camera located 170 cm above the set up (Viewpoint-Behavior technologies). After a 5 min habituation in the smaller compartment, the assay consisted in three successive sessions of 10 min, during which the tested mouse was allowed to explore the total device and the numbers of nose pokes on two pencil boxes were counted. In the first session (habituation), the two boxes were empty. In the second (sociability), one box contained a stranger C57BL/6J (B6) male and the other a lure (a black pebble 37 mm long, 12 mm thick). In the third (social novelty), the C57BL/6J (B6) was left in its box and the lure was replaced by a stranger SWR male. Before the second and the third sessions, the tested mouse was gently pushed into the smaller compartment while positioning the B6 and the SWR conspecifics.

The social interactions were also assessed in a separate series of experiments in *Tshz3*$^{+/lacZ}$ and wild-type mice in a CD-1 background, using the three-chamber test according to the previously reported protocols45,46 but without the automation. Experiments were conducted in male mice, which were group-housed 3-5 per cage from weaning to behavioral testing.

Open field exploration test—Mice were placed at the periphery of a white cylinder (100 cm diameter), divided into three virtual concentric zones of equal surface (150 lux on the ground). The total distance walked, the number of zone crossing and the time spent in the center of the arena were video-recorded for 20 minutes and used respectively to assess ambulatory activity, field of interest and anxiety-like behavior.

Hole board test—Reduced field of interest with repetitive behavior was explored in an automated hole-board. The apparatus consisted of a grey vinyl plastic board (40 x 40 cm) with 16 equidistant holes (3.5cm diameter) forming 4 rows and four columns. Photobeams crossing the holes allowed automatic counts of nose pokes for each hole. The board was located in the center of a room (60 lux). The mouse was always placed in the same corner of the board and allowed to explore for 10 min. We measured the total number of nose dips according to47,48 distinguishing the exploratory dips from the stereotyped dips for each mouse.

Marble burying test—This test relates to pushing and digging behavior and provides a measure of repetitive and perseverating behavior69. The number of covered marbles depends on the frequency of pushing and digging episodes. The cages (40 x 40 x 18 cm) are filled with litter (5 cm thick). After a 10 min habituation period in a new cage, the tested mouse is restricted to a corner of the cage with a mobile partition, while twenty marbles (1 cm in diameter) in 4 evenly spaced rows of 5 marbles are placed on top of the bedding. The partition is removed and the mouse is left alone for 30 minutes. Buried was defined as completely covered by the litter and scored 3; the score 2 corresponded to 2/3 buried and score 1 to 1/2 buried.

Elevated plus-maze—The elevated plus-maze provides a measure of anxiety-like behavior based on the avoidance of a condition generating anxiety. We used a plus-shaped device with two open and two closed arms, elevated 80 cm from the floor. Each mouse was placed in the central area of the maze (6 × 6 cm), with its head towards the enclosed arm, and allowed to move freely for 15 min. The distance travelled (cm) in the opened and closed arms was measured by a video track system.

Sensory functions—We have examined *Tshz3*$^{+/lacZ}$ and wild-type mice for vision, audition and olfaction, since the results obtained in different tasks depend on the integrity of these functions. The mice were subjected to sensorial controls within two weeks after the last experimental testing.

Visual performance: We took the mouse by the tail between the thumb and the forefinger and lifted it. The tip of a pencil was approached to its eyes, without touching the vibrissae. The mouse raised the head, extended the forelimbs and grasped or tried to grasp the pen when the visual function was undamaged. The scores were: raising the head (1), extending the forelimbs (2) and grasping or trying to grasp the pen (3). The task was administered four times at 10 minutes intervals. The score was the sum of the three last trials.

Auditory performance: The Preyer response was used for detecting potential auditory impairment. It consisted in pinna twitching and going flat backwards against the head as reaction to sound. The response was validated as an indicator of the auditory acuity by measuring the associated averaged evoked auditory potential70,71. We evaluated the responses to stimulations in the ultrasound bandwidth. The mice, placed in soundproof chamber, received sounds from two dog whistles (10 cm from the ear). The first produced 50 ± .008 kHz and the second 35 ± .010 kHz sounds. The mouse received 5 stimulations from

each whistle at 3 minutes intervals. The Preyer response was scored 1 for a partial response (ear startling) and 2 for a full response (pinna going flat backwards against the head).

Olfactory capacities: The olfactory habituation/dishabituation test was performed according to the previously described classical protocol72 that measures the capacity to detect and discriminate different odors. Several odors were presented to the mouse on a cotton tip: neutral (water), non-social (synthetic violet and vanilla aromas that were sugar free) and social (urines from B6 and SWR male mice). Each odor was presented three times for two minutes and the time spent in sniffing the cotton tip was recorded. The median of three consecutive trials was calculated for each odor and for each mouse and the score of group was the mean score of the individual median score. The testing room was ventilated and only one mouse was present during the trials.

Supplementary Material

Refer to Web version on PubMed Central for supplementary material.

Acknowledgements

This work was supported by CNRS and Aix-Marseille University to L.KLG., L.F., and M.C., INSERM and Aix-Marseille University to PLR; Fédération pour la Recherche sur le Cerveau (FRC) to L.F.; the National Institutes of Health grants MH103339, MH106934 and MH106874, the Simons Foundation, and the Kavli Foundation to N.S.; the Medical Research Council (MR/L002744/1), the Manchester Biomedical Research Centre and the NIHR Greater Manchester Clinical Research Network to A.S.W. Funding for A.N. Garratt was from the German Federal Ministry for Education and Research (BMBF, NGFN-plus, “Alzheimer Disease Integrative Genomics”, PNA-01GS08127-3a). We thank Cristophe Scajola for taking care of the mice used to study behavior. Microscopy was performed at the imaging platform of IBDM, supported by the French National Research Agency through the “Investments for the Future” program (France-BioImaging, ANR-10-INSB-04-01).

References

1. Association AP. Diagnostic and Statistical Manual of Mental Disorders, DSM-5. Fifth Edition. American Psychiatric Association; Washington, DC: 2013.
2. Buxbaum JD, et al. The autism sequencing consortium: large-scale, high-throughput sequencing in autism spectrum disorders. Neuron. 2012; 76:1052–6. [PubMed: 23259942]
3. Parikshak NN, et al. Integrative functional genomic analyses implicate specific molecular pathways and circuits in autism. Cell. 2013; 155:1008–21. [PubMed: 24267887]
4. State MW, Sestan N. Neuroscience. The emerging biology of autism spectrum disorders. Science. 2012; 337:1301–3. [PubMed: 22984058]
5. Willsey AJ, et al. Coexpression networks implicate human midfetal deep cortical projection neurons in the pathogenesis of autism. Cell. 2013; 155:997–1007. [PubMed: 24267886]
6. Belmonte MK, et al. Autism and abnormal development of brain connectivity. J Neurosci. 2004; 24:9228–31. [PubMed: 15496656]
7. Kwan KY, Sestan N, Anton ES. Transcriptional co-regulation of neuronal migration and laminar identity in the neocortex. Development. 2012; 139:1535–46. [PubMed: 22492350]
8. Rosenfeld JA, et al. Small deletions of SATB2 cause some of the clinical features of the 2q33.1 microdeletion syndrome. PLoS One. 2009; 4:e6568. [PubMed: 19668335]
9. Rosenfeld JA, et al. Copy number variations associated with autism spectrum disorders contribute to a spectrum of neurodevelopmental disorders. Genet Med. 2010; 12:694–702. [PubMed: 20808228]
10. Wang K, et al. Common genetic variants on 5p14.1 associate with autism spectrum disorders. Nature. 2009; 459:528–33. [PubMed: 19404256]

11. O'Roak BJ, et al. Multiplex targeted sequencing identifies recurrently mutated genes in autism spectrum disorders. Science. 2012; 338:1619–22. [PubMed: 23160955]
12. Kang HJ, et al. Spatio-temporal transcriptome of the human brain. Nature. 2011; 478:483–9. [PubMed: 22031440]
13. Ariani F, et al. FOXG1 is responsible for the congenital variant of Rett syndrome. Am J Hum Genet. 2008; 83:89–93. [PubMed: 18571142]
14. Chen B, Schaevitz LR, McConnell SK. Fezl regulates the differentiation and axon targeting of layer 5 subcortical projection neurons in cerebral cortex. P Natl Acad Sci USA. 2005; 102:17184–9.
15. Chen JG, Rasin MR, Kwan KY, Sestan N. Zfp312 is required for subcortical axonal projections and dendritic morphology of deep-layer pyramidal neurons of the cerebral cortex. P Natl Acad Sci USA. 2005; 102:17792–7.
16. Han W, et al. TBR1 directly represses Fezf2 to control the laminar origin and development of the corticospinal tract. P Natl Acad Sci USA. 2011; 108:3041–6.
17. Bedogni F, et al. Tbr1 regulates regional and laminar identity of postmitotic neurons in developing neocortex. P Natl Acad Sci USA. 2010; 107:13129–34.
18. Molyneaux BJ, Arlotta P, Hirata T, Hibi M, Macklis JD. Fezl is required for the birth and specification of corticospinal motor neurons. Neuron. 2005; 47:817–31. [PubMed: 16157277]
19. Leone DP, et al. Satb2 Regulates the Differentiation of Both Callosal and Subcerebral Projection Neurons in the Developing Cerebral Cortex. Cereb cortex. 2014; 25:3406–3419. [PubMed: 25037921]
20. Bishop KM, Garel S, Nakagawa Y, Rubenstein JL, O'Leary DD. Emx1 and Emx2 cooperate to regulate cortical size, lamination, neuronal differentiation, development of cortical efferents, and thalamocortical pathfinding. J Comp Neurol. 2003; 457:345–60. [PubMed: 12561075]
21. Britanova O, et al. Satb2 is a postmitotic determinant for upper-layer neuron specification in the neocortex. Neuron. 2008; 57:378–92. [PubMed: 18255031]
22. A full genome screen for autism with evidence for linkage to a region on chromosome 7q. International Molecular Genetic Study of Autism Consortium. Hum Mol Genet. 1998; 7:571–8. [PubMed: 9546821]
23. Liu J, et al. A genomewide screen for autism susceptibility loci. Am J Hum Genet. 2001; 69:327–40. [PubMed: 11452361]
24. Hussman JP, et al. A noise-reduction GWAS analysis implicates altered regulation of neurite outgrowth and guidance in autism. Mol Autism. 20011; 2:1.
25. Caubit X, et al. Teashirt 3 regulates development of neurons involved in both respiratory rhythm and airflow control. J Neurosci. 2010; 30:9465–76. [PubMed: 20631175]
26. Caubit X, Tiveron MC, Cremer H, Fasano L. Expression patterns of the three Teashirt-related genes define specific boundaries in the developing and postnatal mouse forebrain. J Comp Neurol. 2005; 486:76–88. [PubMed: 15834955]
27. Adalat S, Bockenhauer D, Ledermann SE, Hennekam RC, Woolf AS. Renal malformations associated with mutations of developmental genes: messages from the clinic. Pediatr Nephrol. 2010; 25:2247–55. [PubMed: 20603712]
28. Chowdhury S, et al. Phenotypic and molecular characterization of 19q12q13.1 deletions: a report of five patients. Am J Med Genet Part A. 2014; 164A:62–9. [PubMed: 24243649]
29. Kulharya AS, Michaelis RC, Norris KS, Taylor HA, Garcia-Heras J. Constitutional del(19)(q12q13.1) in a three-year-old girl with severe phenotypic abnormalities affecting multiple organ systems. Am J Med Genet. 1998; 77:391–4. [PubMed: 9632168]
30. Malan V, et al. 19q13.11 deletion syndrome: a novel clinically recognisable genetic condition identified by array comparative genomic hybridisation. J Med Genet. 2009; 46:635–40. [PubMed: 19126570]
31. Kwan KY, et al. SOX5 postmitotically regulates migration, postmigratory differentiation, and projections of subplate and deep-layer neocortical neurons. P Natl Acad Sci USA. 2008; 105:16021–6.
32. Lai T, et al. SOX5 controls the sequential generation of distinct corticofugal neuron subtypes. Neuron. 2008; 57:232–47. [PubMed: 18215621]

33. Li H, et al. Transcription factor MEF2C influences neural stem/progenitor cell differentiation and maturation in vivo. P Natl Acad Sci USA. 2008; 105:9397–402.
34. Novara F, et al. Refining the phenotype associated with MEF2C haploinsufficiency. Clin Genet. 2010; 78:471–7. [PubMed: 20412115]
35. Arlotta P, et al. Neuronal subtype-specific genes that control corticospinal motor neuron development in vivo. Neuron. 2005; 45:207–21. [PubMed: 15664173]
36. Workman AD, Charvet CJ, Clancy B, Darlington RB, Finlay BL. Modeling transformations of neurodevelopmental sequences across mammalian species. J Neurosci. 2013; 33:7368–83. [PubMed: 23616543]
37. Hoerder-Suabedissen A, et al. Expression profiling of mouse subplate reveals a dynamic gene network and disease association with autism and schizophrenia. P Natl Acad Sci USA. 2013; 110:3555–60.
38. Mi H, Poudel S, Muruganujan A, Casagrande JT, Thomas PD. PANTHER version 10: expanded protein families and functions, and analysis tools. Nucleic Acids Res. 2016; 44:D336–42. [PubMed: 26578592]
39. Caubit X, et al. Teashirt 3 is necessary for ureteral smooth muscle differentiation downstream of SHH and BMP4. Development. 2008; 135:3301–10. [PubMed: 18776146]
40. Shepherd GM. Corticostriatal connectivity and its role in disease. Nat Rev Neurosci. 2013; 14:278–91. [PubMed: 23511908]
41. Sohur US, Padmanabhan HK, Kotchetkov IS, Menezes JR, Macklis JD. Anatomic and Molecular Development of Corticostriatal Projection Neurons in Mice. Cereb Cortex. 2012; 24:293–303. [PubMed: 23118198]
42. Arlotta P, Molyneaux BJ, Jabaudon D, Yoshida Y, Macklis JD. Ctip2 controls the differentiation of medium spiny neurons and the establishment of the cellular architecture of the striatum. J Neurosci. 2008; 28:622–32. [PubMed: 18199763]
43. Varlinskaya EI, Spear LP. Acute effects of ethanol on social behavior of adolescent and adult rats: role of familiarity of the test situation. Alcohol Clin Exp Res. 2002; 26:1502–11. [PubMed: 12394283]
44. Roubertoux, PL.; Carlier, M.; Tordjman, S. Organism Models of Autism Spectrum Disorders. Roubertoux, PL., editor. Springer; 2015. p. 335-370.
45. Nadler JJ, et al. Automated apparatus for quantitation of social approach behaviors in mice. Genes Brain Behav. 2004; 3:303–14. [PubMed: 15344923]
46. Moy SS, et al. Sociability and preference for social novelty in five inbred strains: an approach to assess autistic-like behavior in mice. Genes Brain Behav. 2004; 3:287–302. [PubMed: 15344922]
47. Irie F, Badie-Mahdavi H, Yamaguchi Y. Autism-like socio-communicative deficits and stereotypies in mice lacking heparan sulfate. P Natl Acad Sci USA. 2012; 109:5052–6.
48. Makanjuola RO, Hill G, Maben I, Dow RC, Ashcroft GW. An automated method for studying exploratory and stereotyped behaviour in rats. Psychopharmacology. 1977; 52:271–7. [PubMed: 406630]
49. Cohen, J. Statistical Power Analysis for the Behavioral Sciences. Routledge; New York: 1988.
50. Lai MC, Lombardo MV, Baron-Cohen S. Autism. Lancet. 2014; 383:896–910. [PubMed: 24074734]
51. Jenkins D, et al. Analysis of TSHZ2 and TSHZ3 genes in congenital pelvi-ureteric junction obstruction. Nephrol Dial Transplant. 2010; 25:54–60. [PubMed: 19745106]
52. Brandt T, et al. Complex autism spectrum disorder in a patient with a 17q12 microduplication. Am J Med Genet Part A. 2012; 158A:1170–7. [PubMed: 22488896]
53. Handrigan GR, et al. Deletions in 16q24.2 are associated with autism spectrum disorder, intellectual disability and congenital renal malformation. J Med Genet. 2013; 50:163–73. [PubMed: 23335808]
54. Bodria M, Sanna-Cherchi S. Genetic Basis of Congenital Anomalies of the Kidney and Urinary Tract. G Ital Nefrol. 2015; 32(Suppl 64)
55. Mefford, H.; Mitchell, E.; Hodge, J. 17q12 Recurrent Duplication. In: Pagon, RA., et al., editors. GeneReviews. Seattle, WA: University of Washington, Seattle: 2016.

56. O'Leary DD, Koester SE. Development of projection neuron types, axon pathways, and patterned connections of the mammalian cortex. Neuron. 1993; 10:991–1006. [PubMed: 8318235]
57. Delmonte S, Gallagher L, O'Hanlon E, McGrath J, Balsters JH. Functional and structural connectivity of frontostriatal circuitry in Autism Spectrum Disorder. Front Hum Neurosci. 2013; 7:430. [PubMed: 23964221]
58. Peca J, et al. Shank3 mutant mice display autistic-like behaviours and striatal dysfunction. Nature. 2011; 472:437–42. [PubMed: 21423165]
59. Blundell J, et al. Neuroligin-1 deletion results in impaired spatial memory and increased repetitive behavior. J Neurosci. 2010; 30:2115–29. [PubMed: 20147539]
60. Portmann T, et al. Behavioral abnormalities and circuit defects in the basal ganglia of a mouse model of 16p11.2 deletion syndrome. Cell Rep. 2014; 7:1077–92. [PubMed: 24794428]
61. Paxinos, G.; Franklin, KBJ. The mouse brain in stereotaxic coordinates. Second edition. Academic Press; 2001.
62. Kim D, et al. TopHat2: accurate alignment of transcriptomes in the presence of insertions, deletions and gene fusions. Genome Biol. 2013; 14:R36. [PubMed: 23618408]
63. Langmead B, Salzberg SL. Fast gapped-read alignment with Bowtie 2. Nat Methods. 2012; 9:357–9. [PubMed: 22388286]
64. Banerjee-Basu S, Packer A. SFARI Gene: an evolving database for the autism research community. Dis Models Mech. 2010; 3:133–5.
65. Chassain C, et al. Metabolic, synaptic and behavioral impact of 5-week chronic deep brain stimulation in hemiparkinsonian rats. J Neurochem. 2016; 136:1004–16. [PubMed: 26576509]
66. Jiang ZG, North RA. Membrane properties and synaptic responses of rat striatal neurones in vitro. J Physiol. 1991; 443:533–53. [PubMed: 1822537]
67. Beurrier C, et al. Ciliary neurotrophic factor protects striatal neurons against excitotoxicity by enhancing glial glutamate uptake. PLoS One. 2010; 5:e8550. [PubMed: 20062544]
68. IBM Corp. IBM SPSS Statistics for Windows. Version 19.0. Armonk, NY: IBM Corp., Release; 2010.
69. Thomas A, et al. Marble burying reflects a repetitive and perseverative behavior more than novelty-induced anxiety. Psychopharmacology. 2009; 204:361–73. [PubMed: 19189082]
70. Ehret G, Romand R. Development of tone response thresholds, latencies and tuning in the mouse inferior colliculus. Brain Res Dev Brain Res. 1992; 67:317–26. [PubMed: 1511522]
71. Willott, JF. The Auditory Psychobiology of the mouse. Springfield, Ill: Thomas, c1983; 1983. p. 507
72. Yang M, Crawley JN. Simple behavioral assessment of mouse olfaction. Curr Protoc Neurosci. 2009; Ch 8:Unit 8 24.

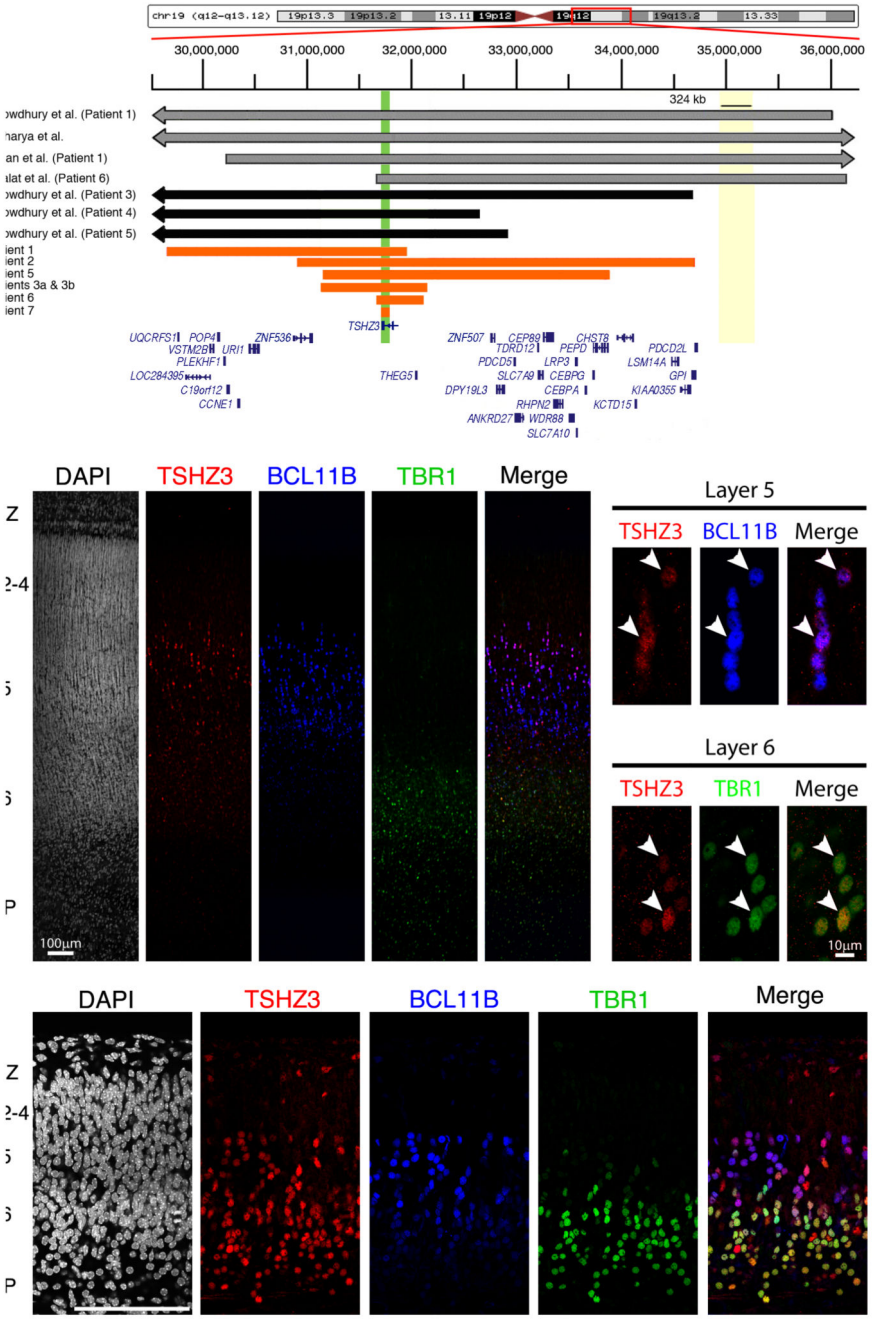

Figure 1. Schematic of deletions of the *TSHZ3* locus and TSHZ3 expression in the human and mouse fetal neocortex

(**a**) An ideogram of chromosome 19 and the relevant interval of 19q12q13.12 are displayed at the top. Horizontal bars represent deletions spanning the *TSHZ3* gene. Orange bars are for individuals from this study. These new cases allow delineating a novel minimal region of overlap (MRO) of approximately 50kb ([hg19] chr19:31,765,881-31,812,396) represented by a vertical green box, which spans the *TSHZ3* gene only. This MRO, which corresponds to the deletion found in patient 7, uncovers the second exon and part of the intron of *TSHZ3*.

Grey and black bars are for published cases deleting *TSHZ3* with or without deletion of a previously described MRO (vertical yellow box) for the syndrome associated with 19q13.11 microdeletions. (**b**) Expression of TSHZ3 (red) and of markers of deep layers cortical neurons BCL11B (blue) and TBR1 (green) in the human cerebral cortex at 20 weeks of gestation and (**c**) in coronal brain sections of the mouse cortex at E18.5. Scale bar = 100 μm in (**b**) and 50 μm in (**c**). L2-6: Cortical layers 2-6; MZ: Marginal zone; SP: Subplate. In b, arrowheads point to double positive cells.

Europe PMC Funders Author Manuscripts

Europe PMC Funders Author Manuscripts

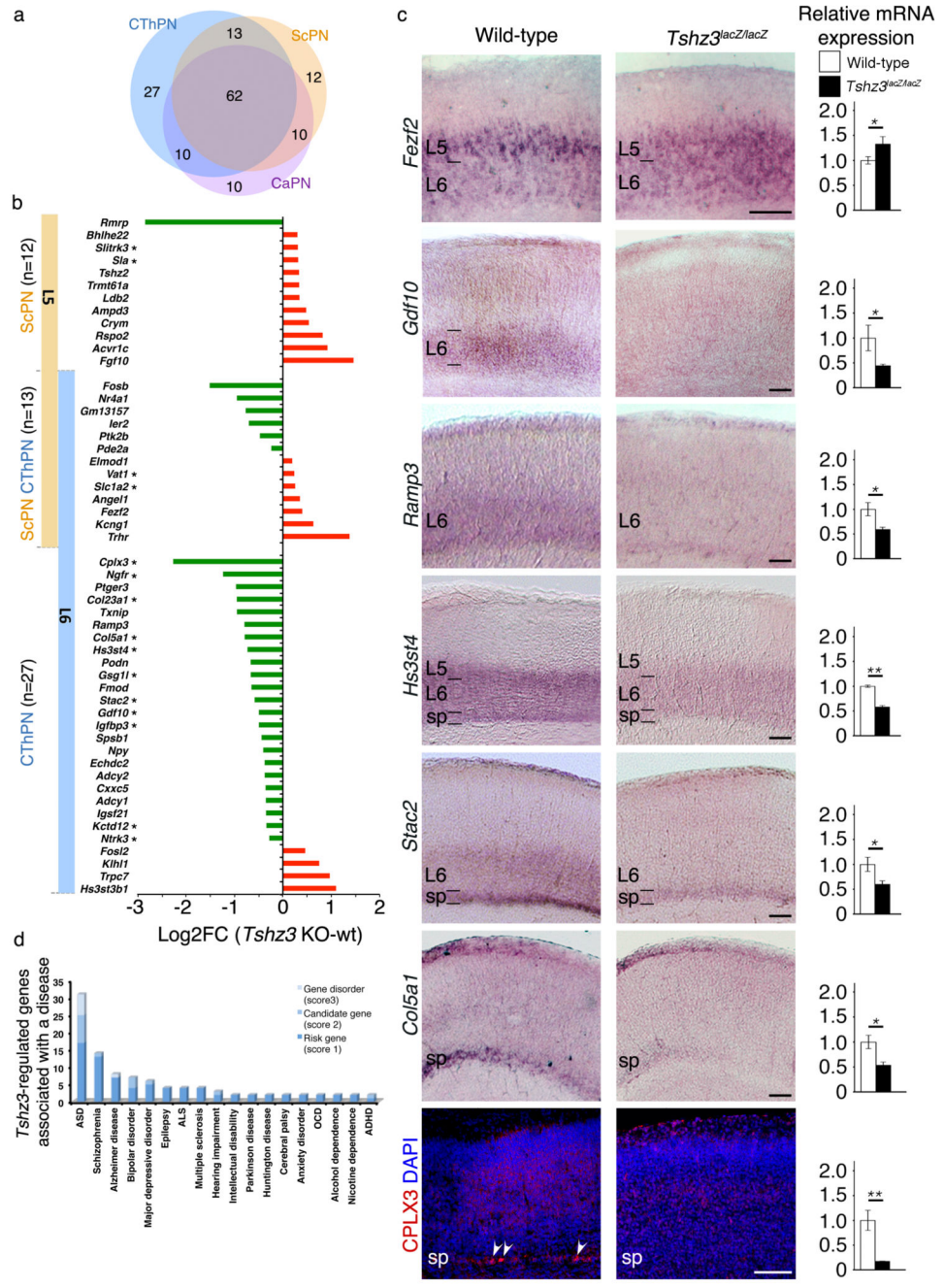

Figure 2. *Tshz3*$^{lacZ/lacZ}$ mice show altered gene expression of cortical layer markers at E18.5

(**a**) Venn diagram identifying the DEX genes common or specific to cortical neuron subtypes (CaPN, callosal projection neurons; CThPN, corticothalamic projection neurons; ScPN, subcerebral projection neurons). (**b**) Fold changes (FC, log2 scale) in the 52 DEX genes that are preferentially expressed in L5 and/or L6 in *Tshz3*$^{lacZ/lacZ}$ cortex vs. wild-type. *indicate genes also expressed in the subplate. (**c**) *In situ* hybridization for selected DEX genes on coronal brain sections (*Fezf2, Gdf10, Ramp3, Hs3st4, Stac2, Col5a1*), CPLX3 immunoreactivity and mRNA level variation ± s.e.m. (n = 3) analyzed by qRT-PCR in

Tshz3$^{lacZ/lacZ}$ versus wild-type mice. Scale bars, 100 μm. * $p<0.05$; ** $p<0.02$ by unpaired two-tailed *t* test. In c, arrowheads point to CPLX3 positive cells. (**d**) Human brain and nervous system pathologies associated with orthologs of the 52 *Tshz3*-regulated DEX genes. Scores: 1, one study; 2, two studies; 3, three or more studies. ADHD: attention deficit/hyperactivity disorder; ALS: amyotrophic lateral sclerosis; ASD: autism spectrum disorder; OCD: obsessive compulsive disorder.

Europe PMC Funders Author Manuscripts

Europe PMC Funders Author Manuscripts

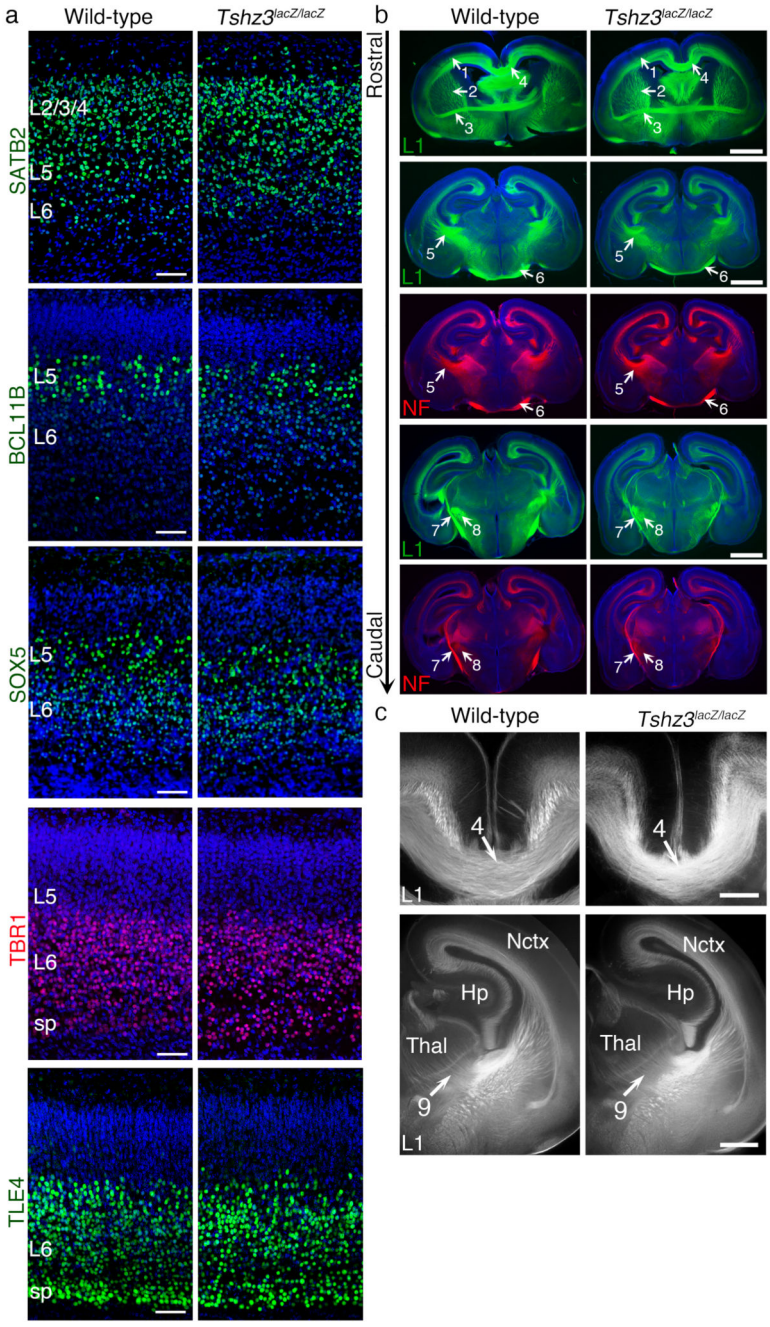

Figure 3. Cortical layering and major axonal tracts are preserved in *Tshz3*$^{lacZ/lacZ}$ brains at E18.5

(**a**) Staining of markers that allow the distinction of cortical layers in coronal brain sections of the mouse cortex at E18.5. DAPI (blue). (**b**) L1-CAM (L1, green) and neurofilament (NF, red) and (**c**) L1-CAM (L1, white) immunostainings of coronal brain sections at E18.5. Numbered arrows point to: (1) fibers in the cortical intermediate zone, (2) striatal axonal bundles, (3) anterior commissure, (4) corpus callosum, (5) internal capsule, (6) optic chiasm,

(7) optic tract, (8) cerebral peduncle, (9) corticothalamic tract. Hp: hippocampus; Nctx: neocortex; Thal: thalamus. Scale bars: 50 μm (a), 1 mm (b) and 0.5 mm (c).

Europe PMC Funders Author Manuscripts

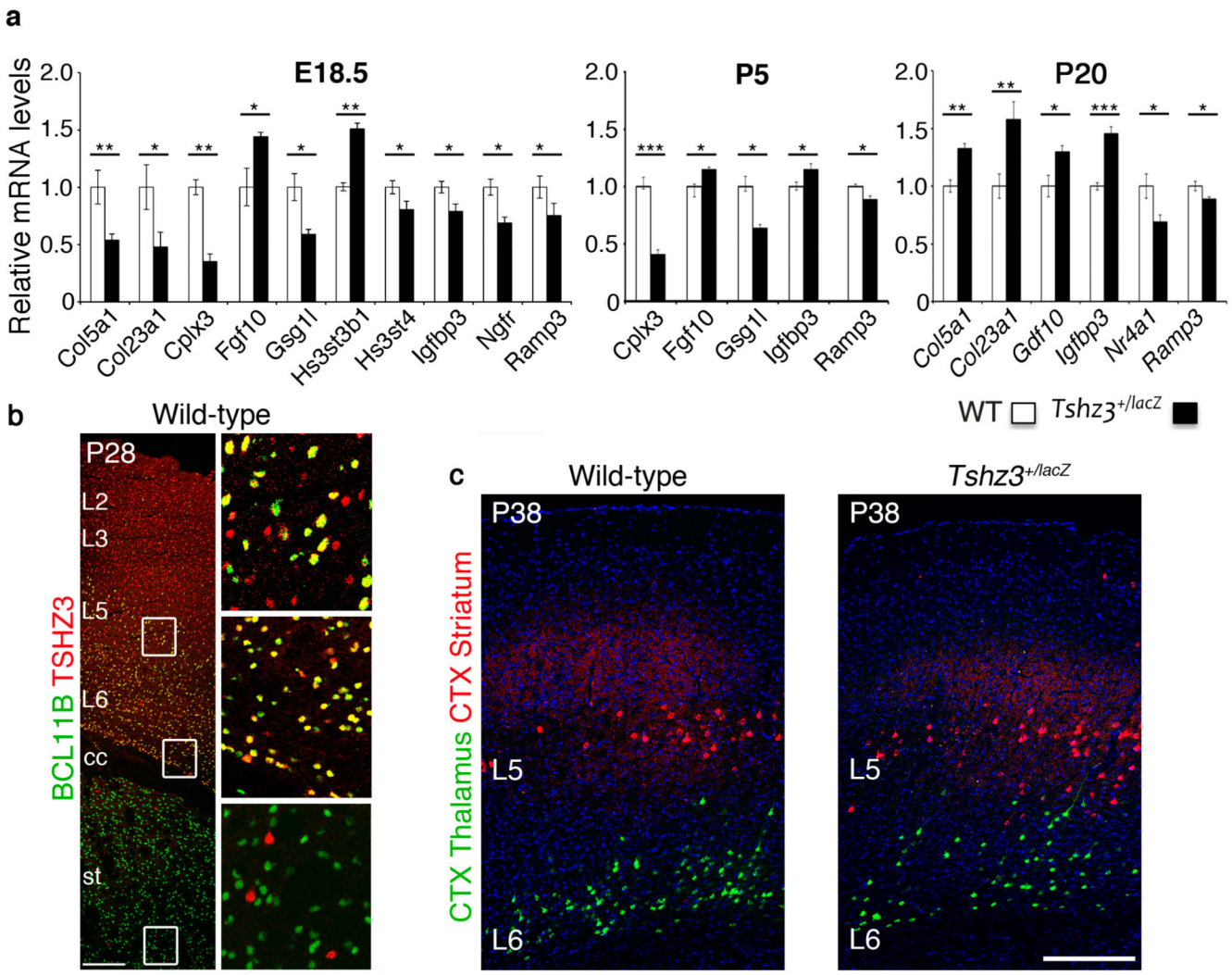

Figure 4. *Tshz3*$^{+/lacZ}$ mice exhibit altered expression of genes in the neocortex from embryonic to postnatal stages but main projection systems from deep CPNs are preserved

(**a**) Quantitative-PCR analyses of DEX genes in the cortex of *Tshz3*$^{+/lacZ}$ (n=6) and wild-type (n=6) at E18.5, P5 and P20. Data are expressed as mean ± s.e.m. * p<0.05; ** p<0.02; *** p<0.005; unpaired *t* test. (**b**) Immunodetection of TSHZ3 (red) and BCL11B (green) in the cortex and the striatum. Boxed regions are magnified. TSHZ3/BCL11B double positive neurons are found in L6 and L5 but not in L2/3. The few TSHZ3 positive cells found in the striatum are not positive for BCL11B, a marker of MSNs. (**c**) Ipsilateral L5 (red) and L6 (green) cortical neurons are labeled 10 days after unilateral injection of cholera toxin B conjugated with Alexa-Fluor 488 into the striatum and conjugated with Alexa Fluor 647 into the thalamus in P28-old wild-type and *Tshz3*$^{+/lacZ}$ mice, showing that the corticostriatal and corticothalamic tracts are present in the mutant and L5/L6 layering is preserved. cc: corpus callosum; st: striatum; WT: wild-type. Scale bars 200 μm.

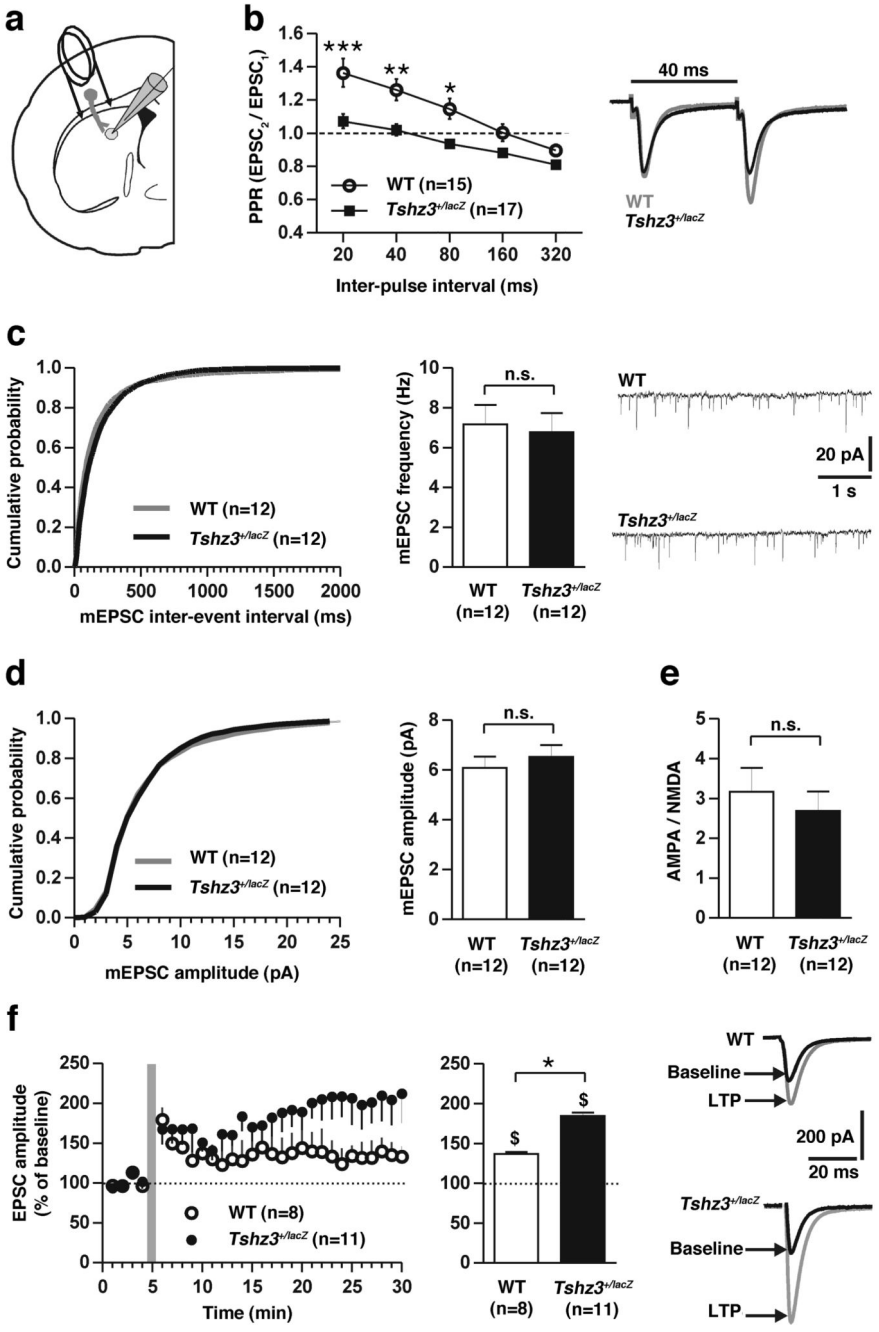

Figure 5. Altered corticostriatal synaptic transmission and plasticity in *Tshz3*$^{+/lacZ}$ mice

(**a**) Scheme of a mouse brain coronal slice with a CPN (dark gray), the stimulating electrode on the corpus callosum and the recording electrode on a striatal MSN (light gray). (**b-f**) Sample sizes (n) refer to the number of recorded MSNs. (**b**) PPR is lower in *Tshz3*$^{+/lacZ}$ compared to wild-type (WT) mice [$F(1,144)=38.7$ (2-way ANOVA); *$p<0.05$, **$p<0.01$, ***$p<0.001$ (Bonferroni post-test)], suggesting increased AP-dependent glutamate release from corticostriatal synapses (traces show samples of 2 consecutive EPSCs normalized to $EPSC_1$). (**c**) mEPSCs frequency (left graph: inter-event interval, $p>0.05$, 2-samples

Kolmogorov-Smirnov test, 5 ms bins; right histogram: average frequency, p>0.05, Mann-Whitney test; traces show samples of mEPSCs) and (**d**) mEPSC amplitude (left graph: p>0.05, 2-samples Kolmogorov-Smirnov test, 1 pA bins; right histogram: p>0.05, Mann-Whitney test), as well as (**e**) AMPA/NMDA ratio, are similar between *Tshz3*$^{+/lacZ}$ and WT mice, suggesting that heterozygous *Tshz3* loss affects neither AP-independent glutamate release from corticostriatal synapses, nor ionotropic glutamate receptor sensitivity on striatal MSNs. (**f**) While corticostriatal LTP is induced in both WT and *Tshz3*$^{+/lacZ}$ mice, this form of synaptic plasticity is significantly enhanced in mutants; left graph shows the time-course of EPSC amplitude (gray bar represents LTP induction protocol); right histogram shows the average EPSC amplitude after LTP induction (values are normalized to baseline; $^{\$}p<0.001$ vs. baseline, *p<0.001, Mann-Whitney test); traces depict sample EPSCs before (black) and after (gray) the induction of LTP in the two groups. Data are expressed as mean ± s.e.m.

Europe PMC Funders Author Manuscripts

Europe PMC Funders Author Manuscripts

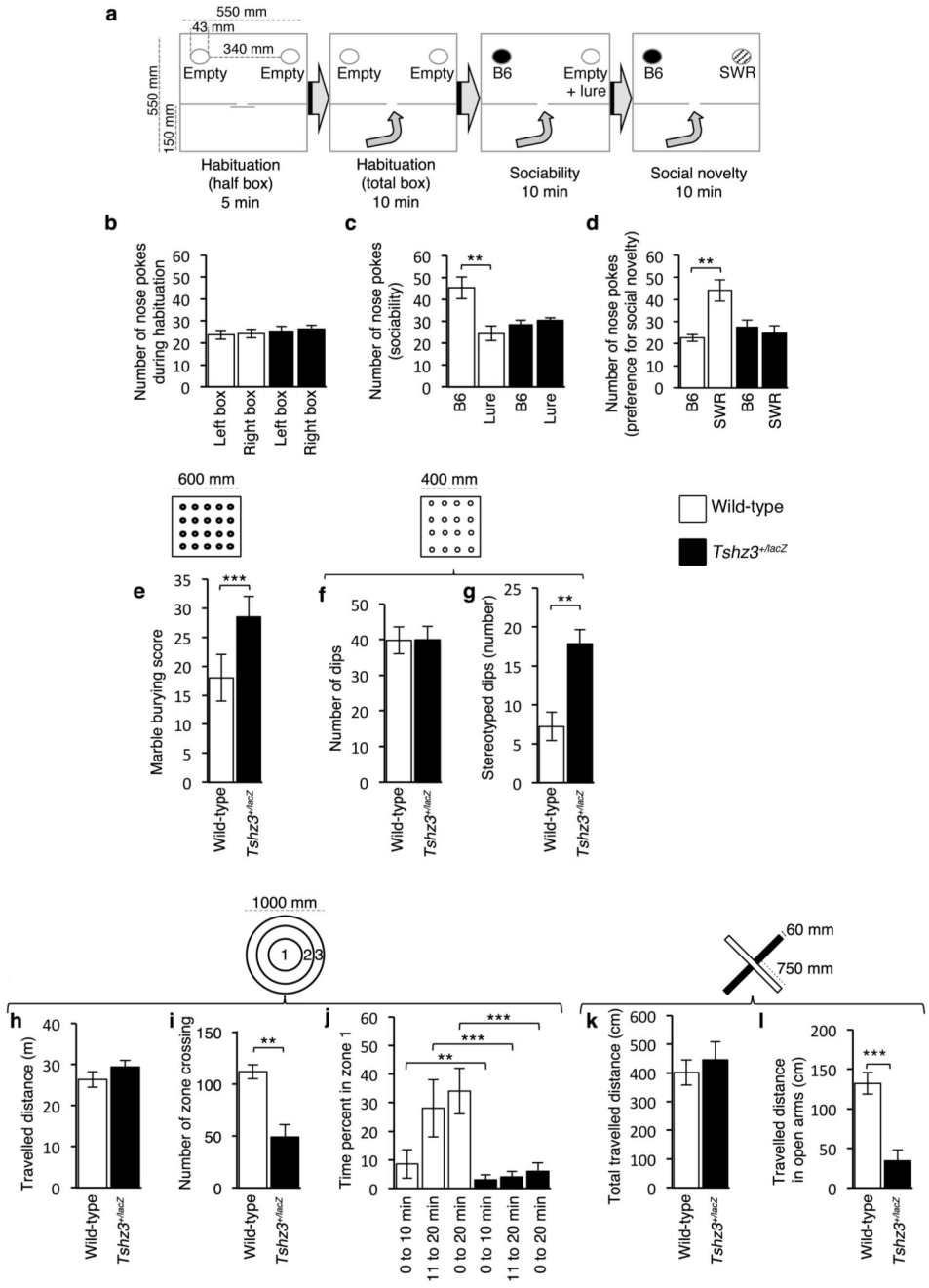

Figure 6. *Tshz3*$^{+/lacZ}$ mice display autism-like behavioral deficits

(**a-d**) **Social behavior**. (**a**) Experimental design. *Tshz3*$^{+/lacZ}$ mice have (**b**) normal activity in habituation, but (**c**) impaired sociability and (**d**) no preference for social novelty. The interaction genotype x sociability x social novelty is significant ($F(1,22) = 39.88$; $p < 0.001$; partial $\eta^2 = 0.64$). The interactions genotype x sociability and genotype x social novelty are significant (ps < 0.001; partial $\eta^2 \geq 0.48$). Unlike wild-type, *Tshz3*$^{+/lacZ}$ do not show higher number of contacts with a stranger B6 vs a lure (wild-type: dependent-t (11) = 4.53; d = 1.31; *Tshz3*$^{+/lacZ}$: dependent-$t < 1$) and with a stranger SWR vs the familiar B6 (wild-type:

dependent-t (11) = 4.42; d = 1.28; *Tshz3*$^{+/lacZ}$: dependent-t (11) = 1.40). **(e-i) Narrowness of the field of interest**. *Tshz3*$^{+/lacZ}$ mice (**e**) bury more marbles (t(22)= 4.77; d = 1.96), (**f**) perform equivalent number of dips but (**g**) perform more stereotyped dips (t(22)= 4.41; d = 1.82). In the open field, *Tshz3*$^{+/lacZ}$ mice (**h**) travel similar distance but (**i**) cross less the zones (t(22) = 3.33; d = 1.36). (**j-l**) **Anxiety-like behavior.** (**j**) *Tshz3*$^{+/lacZ}$ mice spend less time in the open-field central area, with differences in each period (ts(22) ≥ 3.48; ds ≥ 1.17). In the elevated plus-maze, *Tshz3*$^{+/lacZ}$ mice travel (**k**) a similar total distance compared to wild-type (t < 1), but (**l**) a smaller distance in the open arms (t(22) = 5.02; d = 2.05). ** p < 0.001; *** p < 0.0001. Data are mean ± s.e.m. from 12 mice per group.

Europe PMC Funders Author Manuscripts

Europe PMC Funders Author Manuscripts

Table 1

Clinical features of individuals with deletions including *TSHZ3* and/or the critical region characterizing the 19q13.11 deletion syndrome.

Deletion	***TSHZ3* but not the 19q13.11 syndrome critical region**										***TSHZ3* and 19q13.11 syndrome critical region**				**19q13.11 syndrome critical region but not *TSHZ3***							
Patients	**Current study**							**Chowdhury et al. (28)**			**Adalat et al. Family 6 (27)**	**Malan et al. (30)**	**Kulharya et al. (29)**	**Chowdhury (28)**	**Malan et al. (30)**		**Schuurs -Hoeijmakers et al.**	**Gana et al.**		**Chowdhury (28)**	**Forzano et al.**	**Venegas -Vega et al.**
	1	2	3a	3b	5	6	7	Patient 4	Patient 5	Patient 3		Patient 1		Patient 1	Patient 2	Patient 3		Patient 1	Patient 2	Patient 2		
Gender	F	M	M	M	M	F	F	M	F	F	M	M	F	F	M	M	M	M	F	M	F	M
Deletion size (Mb)	2.40	4.02	1.06	1.06	2.87	0.46	0.05	3.91	4.61	6.25	4.5	6.16	11	8.16	4.27	3.19	2.4	1.74	2.63	2.30	1.37	2.49
Inheritance	de novo	de novo	inherited from mother	inherited from mother	de novo	inherited from father	father not tested	de novo	de novo	de novo	father not tested	de novo	father not tested	de novo						de novo		
Phenotypic characteristic																						
Autistic features/ behavioral disorder	stereotypical gesture, attentiveness disorder, echolalia	ASD	atypical autism	ND	hyperactivity, social behavioral deshinibition, graphic dificulties	Autism	ASD		Autism		ASD *											
Renal tract anomalies	Pyelocalyceal dilatation	Nephrolithiasis	-	-	-	-	Vesico-ureteral reflux grade 2	-	-	Congenital hydroureter	Postnatal echogenic kidney **		hydronephrosis	-						-		
Postnatal growth retardation	+	-	+	+	-	-	-	+	+	+	+	+	+	+	+	+	+	+	+	+	+	+
Birth weight; size defect	-	-	-	-	-	-	-	-	+	+	+	+	+	+	+	+	+	+	+	+	+	+
Slender habitus	-	-	-	+	-	-	+	-	-	-	+	+	+	–	+	+	–	+	–	–	+	+
Intellectual disability	cognitive dysexecutive trouble, reasoning trouble, limitations in adaptive behaviour	+	-	-	+	too early to test	cognitive impairment	DD or ID	DD or ID	DD or ID	cognitive impairment	+	+	+	+	+	+	+	+	+	+	+
Other neurologic features	memory deficit	seizures that required anti-epileptic drugs					autoagressive behavior requiring neuroleptics	Wide-based gait	high pain threshold, atypical febrile seizures, normal EEG	–				poor articulation						febrile seizures	one febrile seizure	one febrile seizure
Developmental delay	speech delay	absence of speech	+	-	speech delay	speech delay	speech delay	speech delay	speech delay	speech delay	speech delay	absence of speech	absence of speech	speech delay	speech disturbance	speech disturbance	speech disturbance	speech disturbance	speech disturbance	speech delay	speech disturbance	speech disturbance
Neonatal feeding difficulty	+	-	+	+	-	+	+	+	+	+	+	+	+	+	+	+	+	-	-	+	+	+

Europe PMC Funders Author Manuscripts

Deletion	***TSHZ3* but not the 19q13.11 syndrome critical region**										***TSHZ3* and 19q13.11 syndrome critical region**				**19q13.11 syndrome critical region but not *TSHZ3***							
Patients	**Current study**							**Chowdhury et al. (28)**			**Adalat et al. Family 6 (27)**	**Malan et al. (30)**	**Kulharya et al. (29)**	**Chowdhury (28)**	**Malan et al. (30)**		**Schuurs -Hoeijmakers et al.**	**Gana et al.**		**Chowdhury (28)**	**Forzano et al.**	**Venegas -Vega et al.**
Fifth finger clinodactyly	-	-	-	-	-	-	+	+	-	-	+	+	+	−	+	+	+	+	−	−	+	+
Core clinical features of patients with 19q13.11 deletion syndrome																						
Aplasia cutis in midline of scalp	-	-	-	-	+	-	-	-	-	-	+	+	+	-	+	+	+	+	-	+	+	+
Hair/eyebrows/ eyelashes anomalies	-	-	-	-	-	-	-	-	-	-	+	+	−	−	+	+	+	+	+	−	+	+
Microcephaly	-	-	-	-	-	-	-	-	-	-	+	+	+	+	+	+	+	+	+	+	+	+
Male hypospadias	NA	-	-	-	-	NA	NA	-	NA	NA	−	+	NA	NA	+	+	+	+	NA	+	NA	+
IUGR	-	-	-	-	-	-	-	-	+	-	+	+	+	−	+	+	+	+	+	+	+	NA

+, feature present; -, feature absent; ASD: autism spectrum disorder; Blank spaces correspond to data not documented; DD, developmental disorder; EEG, electroencephalogram; F, female; ID, intellectual disability; IUGR, intrauterine growth retardation; M, male; NA, not applicable; ND, not determined; WG, week of gestation.

ASD diagnosed upon follow up

postnatal imaging revealed bilateral short, echogenic kidneys with the left side contributing 87% function.

Table 1-only References:

H. Schuurs-Hoeijmakers et al., Refining the critical region of the novel 19q13.11 microdeletion syndrome to 750 Kb. *J. Med. Genet.* **46**, 421 (2009).

Gana et al., 19q13.11 cryptic deletion: description of two new cases and indication for a role of WTIP haploinsufficiency in hypospadias. *Eur. J. Hum. Genet.* **20**, 852 (2012).

Forzano et al., 19q13 microdeletion syndrome: Further refining the critical region. *Eur. J. Med. Genet.* **55**, 429 (2012).

Venegas-Vega et al., 19q13.11 microdeletion concomitant with ins(2;19)(p25.3;q13.1q13.4)dn in a boy: potential role of UBA2 in the associated phenotype. *Mol. Cytogenet.* **7**, 61 (2014).